

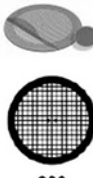
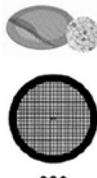

Nanocharacterization by TEM and AFM

We offer a wide range of TEM and AFM tools, from TEM grids and finders to AFM substrates and grippers.

Available in a wide variety of designs and materials to support your work, select from a broad range of mesh sizes, specimen supporting films, and materials that perfectly suit the conditions of your TEM analysis.


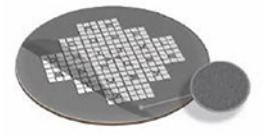
TEM grid specifications:

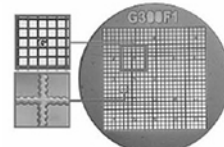
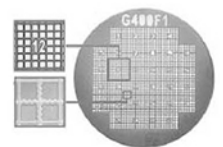
Material	Mesh Size and Shape	Film Specifications
<ul style="list-style-type: none"> • Cu • Ni • Au • Mo • Cu/Pd 	<ul style="list-style-type: none"> • Square or hexagonal • Single-hole grid (75 mm or 100 mm) • 100 • 150 • 200 • 300 • 400 	<ul style="list-style-type: none"> • None • Continuous formvar film (thicknesses: 5-6 nm, 10 nm) • Lacey carbon film (average hole sizes: 50 nm, 100 nm, 150 nm, 100 nm, 150 nm) • Continuous amorphous carbon film (thicknesses: 10 nm, 20-30 nm) • Continuous formvar/carbon film (thickness: 10nm formvar and 1nm carbon)

TEM finder grid specifications:

Material	Mesh Size	Film Specifications
<ul style="list-style-type: none"> • Cu • Ni • Au 	<ul style="list-style-type: none"> • 135 • 200 • 300 • 400 	<ul style="list-style-type: none"> • None • Continuous amorphous carbon film (thicknesses: 3-4 nm, 10 nm, 20-30 nm)

Supporting Tools for Nanomaterial Characterization

Our comprehensive range of supporting materials for nanomaterial characterization includes tweezers (sharp tip, disc gripper for AFM), TEM window grids (various thicknesses, 1 or 9 windows), a magnetic pick-up tool, a grid storage box, cryo-capsules, lift-out grids (Cu or Mo), AFM substrates (various dimensions), and much more.



Explore our complete range of TEM grids on:
SigmaAldrich.com/nanocharacterization

© 2022 Merck KGaA, Darmstadt, Germany and/or its affiliates. All Rights Reserved. Merck, the vibrant M, and Sigma-Aldrich are trademarks of Merck KGaA, Darmstadt, Germany or its affiliates. All other trademarks are the property of their respective owners. Detailed information on trademarks is available via publicly accessible resources.

MK_AD9792EN 43729 08/2022

The Life Science business of Merck operates as MilliporeSigma in the U.S. and Canada.

Sigma-Aldrich®
 Lab & Production Materials

Optimization of Edge Quality in the Slot-Die Coating Process of High-Capacity Lithium-Ion Battery Electrodes


Sandro Spiegel,* Alexander Hoffmann, Julian Klemens, Philip Scharfer, and Wilhelm Schabel

Understanding and reducing edge elevations at the lateral edges are crucial aspects to reduce reject rates during electrode production for lithium-ion batteries (LIB). Herein, different process conditions to reduce edge elevations at the lateral edges of water-based, shear-thinning coatings in the production of LIB electrodes are presented. The reduction of edge elevations is transferred from state-of-the-art electrodes to high-capacity electrodes. The developed process configuration greatly reduces reject caused by cutting off the edge areas in the industrial roll-to-roll process for electrode production. Compared with state-of-the-art electrodes, the reject rate for high-capacity electrode production is significantly higher because the edge geometry in crossweb direction of the electrodes is wider. An optimization can be achieved by a combined adjustment of the coating gap and the slot-die angle to the substrate (angle of attack) to affect the pressure field in the coating bead. Therefore, a systematic investigation and optimization of these process parameters are presented. In addition, the investigation of the process stability of the coating is required. Based on this optimization, a reduction of edge elevations for high-capacity electrode coatings (5 mAh cm^{-2}) of 69% and ultrathick high-capacity electrode coatings (7 mAh cm^{-2}) of 48% is possible.

1. Introduction

Ultrathick electrodes are a promising strategy to increase the ratio of active to passive material and, thus, increase the energy density of battery cells.^[1] In addition, further advantages are saving material and production costs.^[2,3] There are still challenges in processing high-capacity cells with ultrathick electrodes, such as the limited ampacity (current-carrying capacity) and optimizing

S. Spiegel, A. Hoffmann, J. Klemens, P. Scharfer, W. Schabel
Thin Film Technology (TFT)
Material Research Center for Energy Systems (MZE)
Karlsruhe Institute of Technology (KIT)
76131 Karlsruhe, Germany
E-mail: sandro.spiegel@kit.edu

 The ORCID identification number(s) for the author(s) of this article can be found under <https://doi.org/10.1002/ente.202200684>.

© 2022 The Authors. Energy Technology published by Wiley-VCH GmbH. This is an open access article under the terms of the Creative Commons Attribution-NonCommercial-NoDerivs License, which permits use and distribution in any medium, provided the original work is properly cited, the use is non-commercial and no modifications or adaptations are made.

DOI: 10.1002/ente.202200684

the coating and drying steps. The main challenges in coating and drying are edge elevations, process handling, binder migration, and the processing of water-based formulations, especially for cathodes.^[1,4–12]

Edge elevations occur during slot-die coating at the beginning of the process chain of electrode production. Slot-die coating is a premeasured process and state of the art in large-scale battery-cell production.^[13] After the mixing step, the electrode coating is applied to the current collector and dried in a slot-nozzle floatation dryer. After calendaring, the electrodes are cut to size, stacked or rolled, and assembled into cells. Before or after cell assembly, there is typically a postdrying process to remove residual moisture.^[14] In the process chain, the quality of the electrodes and battery cells depends on the previous step. Therefore, the coating step and, in particular, the quality of the wet electrode coating have a great influence on all the subsequent process steps. Consequently, slot-die coating with a high accuracy of wet films in crossweb

direction is scientifically well investigated in literature.^[15–17] Especially, the design of the lips and the cavities of slot dies are thoroughly studied.^[16,18] Due to the complexity of the design possibilities, there is typically one slot-die design for a special application. In comparison with the well-known coating defects such as air entrainment, low-flow limit, barring, or swelling, less scientific research has been published on the subject of edge formation during coating of lithium-ion battery (LIB) electrodes, although edge elevations can cause damage to electrodes or even cell production machines. On the one hand, examples of defects include an accumulation of edge elevations during winding of the dry electrodes. On the other hand, wrinkle formation, cracking, and inhomogeneous porosity distribution occur at the lateral edges of the electrodes due to an inhomogeneous stress distribution in crossweb direction during calendaring.^[15,19,20] These defects lead to production reject and increase production costs and investment. To avoid defects due to undesired edge elevations, cutting off the edges is state of the art in today's large cell production, which also leads to production reject.^[15,21,22] Therefore, it is advisable to prevent edge formation at the lateral edges of the coating already during the coating step before drying. Cutting-edge elevations are schematically shown in Figure 1a.

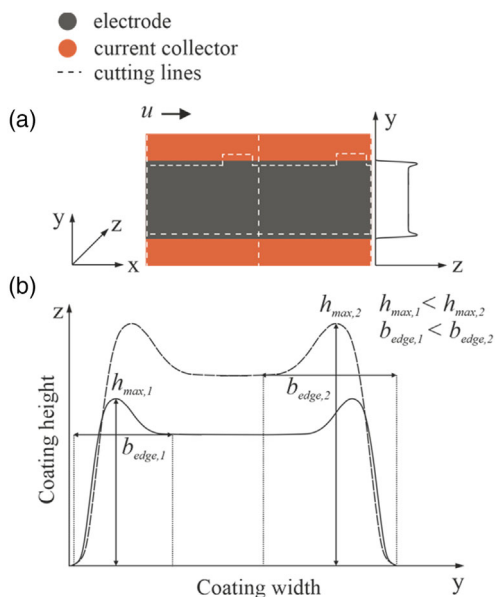


Figure 1. Schematic illustration of a) exemplary electrode cutting and b) edge elevations of electrode coatings.

The reject rate will increase for thick high-capacity electrodes because of wider lateral edges (Figure 1b). This is a major challenge, especially for aqueous anodes and for future aqueous cathode systems with high surface tension. Common theories declare the neck-in flow, which occurs when the fluid leaves the coating bead below the slot die, and surface tension to be the main reasons for the formation of edge elevations.^[10,15,16,19,23] As shown in **Figure 2**, the neck-in flow and resulting edge elevations and the velocity profile of the fluid below the downstream lip are shown.

Both the neck-in flow and high surface tension result in a flow directed toward the center of the coating, forming edge elevations (Figure 2a). Depending on the processing speed, there is a combined mechanism of neck-in flow and surface tension with a higher or lower proportion of the surface tension influence. According to literature, for low-viscosity fluids and low coating speeds, surface tension is a major influence, whereas the influence of coating flow is predominant for high-viscosity battery slurries and high coating speeds.^[19,23] Then, the draw ratio of coating speed u and average flow velocity \bar{u}_{slurry} in the coating gap ($u/\bar{u}_{\text{slurry}}$) is dominant (Figure 2b). If the wet film thickness h_{wet} decreases for a constant coating gap h_G or the coating gap h_G increases for a constant wet film thickness h_{wet} , the draw ratio of coating speed and average flow velocity in the coating gap increases. According to the theory, this leads to an increasing neck-in flow and pronounced edge elevations.^[10,15,19,23]

First, to study and interpret the results, geometric knowledge of the wet film height profiles observed in the work is required. The typical profile is schematically shown in **Figure 3**.

In Figure 3, a usual wet film height profile is shown. Edge elevations with an edge height h_{max} end in a height plateau in the center of the wet film h_{wet} . For the target case of the wet film, height profile without edge elevations $h_{\text{max}} = 0$. In addition, the widening of the coating b_{widening} during the coating process as

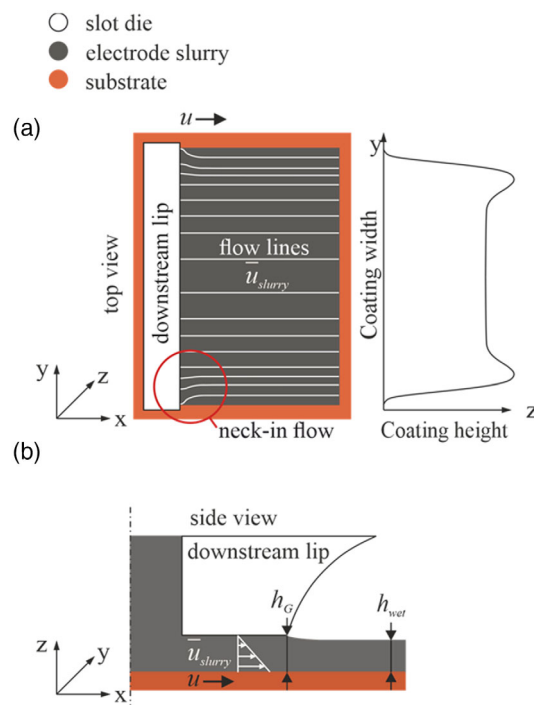


Figure 2. Schematic illustration of the top view of a slot die and the neck-in flow with a) resulting edge elevations and b) the velocity profile of the fluid below the downstream slot-die lip. Reproduced with permission under the terms of the Creative Commons CC BY license.^[1] Copyright 2021, the Authors. Published by Springer Nature.

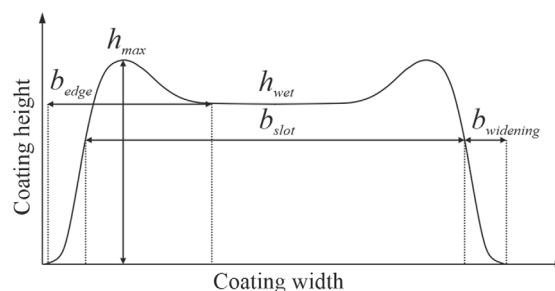


Figure 3. Wet film height profile with geometrical parameters.

well as the outlet width of the slot die b_{slot} and the edge width b_{edge} is shown. For the target case of the wet film height profile without edge elevations $b_{\text{edge}} \rightarrow 0$.

According to Dobroth et al., the dimensionless edge height H^* is defined by the quotient of the edge elevation h_{max} and the average wet film height of the plateau h_{wet} , as shown in Equation (1).^[23]

$$H^* = \frac{h_{\text{max}}}{h_{\text{wet}}} \quad (1)$$

In addition, experiments with different coating gaps can be compared using the known dimensionless coating gap G^* from

the quotient of the coating gap h_G and the average wet film height of the plateau h_{wet} as shown in Equation (2).

$$G^* = \frac{h_G}{h_{wet}} \quad (2)$$

The dimensionless numbers can be calculated with measured values of the wet film height profile and given parameters of the different electrode coatings. Therefore, the parameters of the electrode configurations are listed in **Table 1**.

Coating gap, film thickness, and area weight result from the specification of the target area capacity of the dry electrodes. These parameters are valid for the used electrode slurry (**Table 2**).

In literature, there are some approaches for reducing edge elevations. Schmitt et al. found that for electrode wet film thicknesses smaller than state-of-the-art electrode thicknesses ($h_{wet} \leq 128 \mu\text{m}$), it is possible to eliminate edge elevations during the coating step by equalizing the coating gap h_G and the wet film thickness h_{wet} .^[10,15] Spiegel et al. have shown that this is also valid for state-of-the-art electrode coatings ($h_{wet} \leq 156 \mu\text{m}$).^[1] However, equalizing h_G and h_{wet} is disadvantageous in coating technology because the substrate thickness variations in single-digit micrometer range can lead to undesired wetting of the upper part of the slot-die lips by fluid, which can result in defects such as barring or ribbing.^[16]

Another existing method is the adjustment of the edge area with a specific inner slot-die geometry.^[1,24] By adjusting the internal geometry, the local volume flow at the lateral edges of the coating and, thus, the neck-in flow are reduced. In the work of Spiegel et al., edge elevations could be eliminated for state-of-the-art electrode coatings ($h_{wet} = 156 \mu\text{m}$) by optimizing internal slot-die geometries without adjusting the coating gap.^[1] The adaptation of the internal geometry is limited; if the adaptation of the geometry is too strong, flow defects will occur at the edge area. As the edge elevations of high-capacity electrode coatings are higher compared with state-of-the-art electrode coatings, it is necessary to identify further influencing process parameters. The investigation of the angle of attack of the slot die is promising, as this method can influence the pressure drop and flow

Table 1. Parameters of the different investigated electrode coatings.

Coating gap h_G [μm]	Wet film thickness h_{wet} [μm]	Area weight [g m^{-2}]	Area capacity [mAh cm^{-2}]
420	365	208	7.0
300	260	148	5.0
180	156	90	2.2

Table 2. Composition of the graphite anode slurry.

Components	Dry mass [wt%]
Graphite	93.0
Carbon black	1.40
CMC	1.87
SBR	3.73

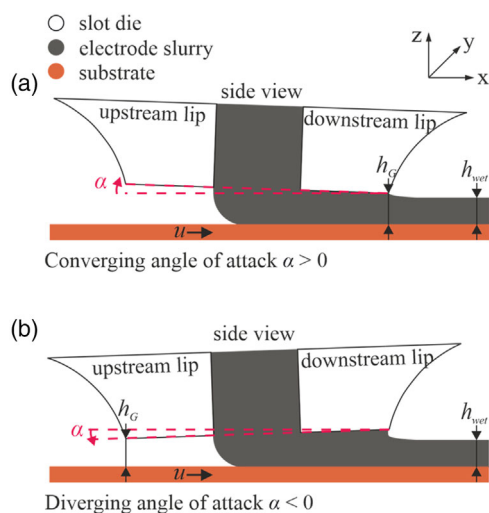


Figure 4. Setting options for the angle of attack α of the slot die a) converging and b) diverging. Reproduced with permission under the terms of the Creative Commons CC BY license.^[1] Copyright 2021, the Authors. Published by Springer Nature.

velocity in the coating gap.^[25–27] In **Figure 4**, the setting options for the angle of attack α of the slot die are shown.

The setting is differentiated into a converging angle of attack $\alpha > 0$, at which the coating gap h_G increases against x -direction (Figure 4a), and a diverging angle of attack $\alpha < 0$, at which the coating gap h_G increases in x -direction (Figure 4b). For both the setting options, the lowest point of the slot-die lips is the fixed coating gap h_G that is set. During slot-die coating, there is a widening of the coating in crossweb direction below the slot-die lips. The widening of the coating is a function of both the coating gap h_G and the angle of attack α . It is expected that for a setting without angle of attack α , this widening is a function of the coating gap h_G . An increasing pressure drop due to a decreasing coating gap h_G below the slot-die lips leads to an increasing widening of the coating in crossweb direction.^[15,28] If the angle of attack α is adapted, both influences take place and the relationship between pressure drop below the upstream die lip and pressure drop below the downstream die lip is decisive. If the pressure drop below the downstream die lip is higher than the pressure drop below the upstream die lip, the widening of the coating increases. This is the case for a converging angle of attack α . This widening could counteract the formation mechanisms of the lateral edge elevations during the coating step (neck-in flow and surface tension) and the edge elevations could decrease. A diverging angle of attack α should have the opposite effect. In addition, it is expected that a lower pressure drop below the upstream die lip at a converging angle of attack α will have a negative effect on defect swelling. Lee et al. have been able to show this effect numerically for different slot-die lip configurations.^[26] Therefore, the degree of the angle of attack α is probably limited by the coating defect swelling.

2. Results and Discussion

In this work, the focus is on investigating the influence of different process parameters such as coating gap h_G and angle

of attack α on the formation of edge elevations during the coating step and process stability. In addition, suitable combinations of the individual influences of process parameters are investigated to reduce edge elevations. All the different influences of process parameters were compared with a standard coating process with a set coating gap ratio $h_G/h_{\text{wet}} = 1.15$ with an angle of attack $\alpha = 0$. The overall aim is to eliminate edge elevations during the coating step.

2.1. Influence of the Coating Gap on Edge Formation

For processing high-capacity electrodes and ultrathick high-capacity electrodes, higher wet film thicknesses ($h_{\text{wet}} = 260\text{--}365\ \mu\text{m}$) are required. In addition to further data for state-of-the-art electrode coatings, experimental data for high-capacity electrode coatings and ultrathick high-capacity electrode coatings were investigated. For this purpose, a constant coating speed of $10\ \text{m}\ \text{min}^{-1}$ was set according to the procedure described in Section 4, and the dimensionless gap G^* was varied. The dimensionless edge height H^* for different electrode coatings and different coating gaps h_G is shown in Figure 5 as a function of the dimensionless coating gap G^* .

The dimensionless edge height H^* of the wet film increases with increasing dimensionless coating gap G^* for the investigated coating gaps h_G . The experimental datasets for different coating gaps h_G are shifted almost in parallel, considering the standard deviation. Thereby, the dimensionless edge height H^* increases with increasing set coating gap h_G ($180\text{--}420\ \mu\text{m}$) comparing constant dimensionless coating gaps G^* . For the coating gap h_G used for state-of-the-art electrode coatings ($h_G = 180\ \mu\text{m}$), a reduction of edge elevations of the wet film via adjustment of the dimensionless coating gap G^* to $\approx 3\ \mu\text{m}$ ($G^* = 1.03$) is possible with regard to $9\ \mu\text{m}$ at a common set G^* of 1.15. For the coating gaps h_G used for thick electrode

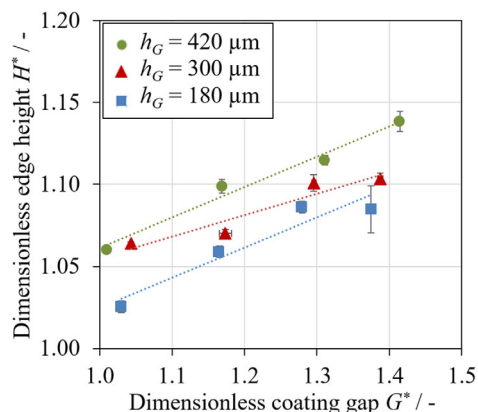


Figure 5. Dimensionless edge height H^* for different electrode coatings and different coating gaps h_G as a function of the dimensionless coating gap G^* . Experimental data of the coating gap h_G used for state-of-the-art electrode coatings ($h_G = 180\ \mu\text{m}$, blue squares), the coating gap h_G used for thick electrode coatings ($h_G = 300\ \mu\text{m}$, red triangles), and the coating gap h_G used for ultrathick electrode coatings ($h_G = 420\ \mu\text{m}$, green dots) are compared for a coating speed of $10\ \text{m}\ \text{min}^{-1}$ (for electrode configurations, see Table 1).

coatings and ultrathick electrode coatings, the reduction of edge formation only via G^* is limited. The edge elevations of thicker electrode coatings ($h_G = 300\ \mu\text{m}$) can be reduced by 23% from $24.0\ (G^* = 1.17)$ to $18.4\ \mu\text{m}\ (G^* = 1.04)$. For ultrathick electrode coatings ($h_G = 420\ \mu\text{m}$), a reduction by 45% from $45.7\ (G^* = 1.17)$ to $25.1\ \mu\text{m}\ (G^* = 1.01)$ is possible. As already known in literature, the influence of the dimensionless gap G^* mitigates the formation of edge elevations.^[1,10,15] A decreasing dimensionless gap G^* results in a decreasing draw ratio of coating speed and average flow velocity below the die lips. This counteracts the neck-in flow and surface tension mechanism in edge formation and leads to decreasing fluid flow inwards the center of the coating. Hence, the dimensionless edge heights H^* and absolute values of the edge elevation decrease.

In addition to the dimensionless edge height H^* , the interpretation of the edge width b_{edge} and the widening of the wet film b_{widening} during the coating process are of interest. In each case, the edge width b_{edge} (Figure 6a) and the widening of the coating during the coating process b_{widening} (Figure 6b) for different

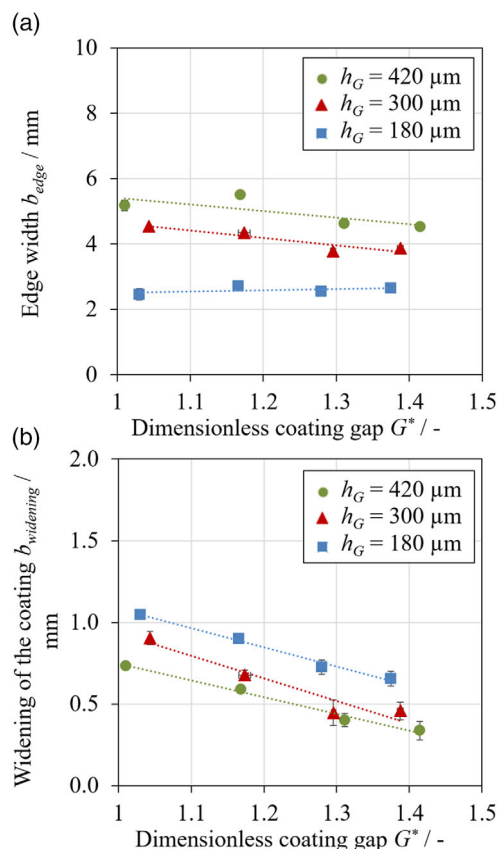


Figure 6. a) Edge width b_{edge} and b) widening of the coating during the coating process b_{widening} for different electrode coatings and different coating gaps h_G as a function of the dimensionless coating gap G^* . Experimental data of the coating gap h_G used for state-of-the-art electrode coatings ($h_G = 180\ \mu\text{m}$, blue squares), the coating gap h_G used for thick electrode coatings ($h_G = 300\ \mu\text{m}$, red triangles), and the coating gap h_G used for ultrathick electrode coatings ($h_G = 420\ \mu\text{m}$, green dots) are compared for a coating speed of $10\ \text{m}\ \text{min}^{-1}$ (for electrode configurations, see Table 1).

electrode coatings and different coating gaps h_G are shown in Figure 6 as a function of the dimensionless coating gap G^* .

The edge width b_{edge} (Figure 6a) of the wet film decreases slightly for all the datasets except the state-of-the-art electrode coating with increasing dimensionless coating gap G^* . The edge width b_{edge} increases with increasing coating gap h_G (180–420 μm) comparing constant dimensionless coating gaps G^* . The widening of the coating during the coating process b_{widening} (Figure 6b) decreases for all the set coating gaps h_G with increasing dimensionless coating gap G^* . For the widening of the coating during the coating process b_{widening} , the experimental values for thicker electrode coatings ($h_G = 420 \mu\text{m}$) are shifted to lower values compared with thinner electrode coatings ($h_G = 180 \mu\text{m}$) for constant dimensionless coating gaps G^* . In addition to reducing the draw ratio, the widening of the coating b_{widening} has an additional influence on edge formation. This effect ensures that the edge elevation is distributed over a larger area in crossweb direction. Due to mass conservation, the widening of the coating counteracts the edge formation effects such as neck-in flow and surface tension. This is supported by the fact that with increasing widening, the dimensionless edge height H^* decreases. Important to know is the critical setting of dimensionless coating gap G^* to 1. In principle, defect-free coating is possible at this operation point, but it could lead to wetting of the upper part of the slot-die lips if the variation of the substrate thickness is too strong. Thus, the substrate thickness variation could reduce the dimensionless coating gap $G^* < 1$, which can lead to inhomogeneous wet films (e.g., barring or ribbing). Therefore, to reduce the edge elevations during slot-die coating for high-capacity electrode coatings or state-of-the-art electrode coatings, other influencing factors must be considered.

2.2. Influence of the Angle of Attack of the Slot Die on Edge Formation

To investigate the influence of the angle of attack α on the coating process, first, the process limits were determined at various angles of attack.

2.2.1. Process Limits

The maximum wet film thickness h_{wet} for different coating gaps h_G as a function of the angle of attack α is shown in Figure 7. As explained in Section 2.1, a decreasing dimensionless coating gap G^* has a negative influence on edge formation. Therefore, an investigation of the lower process limit (minimum wet film thickness) is negligible. The focus is on the investigation of the upper process limit swelling. The wet film thickness h_{wet} was increased for each angle of attack α and coating gap h_G until swelling was observed.

As expected from literature, the maximum wet film thickness h_{wet} decreases with increasing angle of attack α (diverging $< 0 <$ converging) for all the investigated coating gaps h_G . In addition, the experimental data points of the maximum wet film thickness h_{wet} for different coating gaps h_G are approximately shifted in parallel to higher values for increasing coating gap h_G . This is also known from literature for a straight setting of the slot die

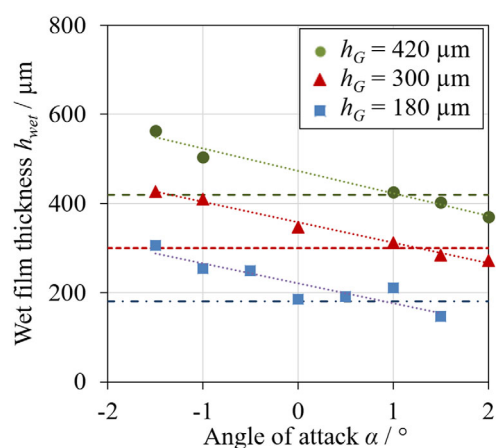


Figure 7. Maximum wet film thickness h_{wet} for different coating gap h_G settings for the investigated electrode thicknesses as a function of the angle of attack α . Experimental data of a coating gap for state-of-the-art electrode coatings ($h_G = 180 \mu\text{m}$, blue squares), a coating gap for thick electrode coatings ($h_G = 300 \mu\text{m}$, red triangles), and a coating gap for ultrathick electrode coatings ($h_G = 420 \mu\text{m}$, green dots) are compared for a coating speed of 10 m min^{-1} (for electrode configurations, see Table 1).

(Section 1). The converging angle of attack $\alpha > 0$ leads to a lower pressure drop below the upstream slot-die lip, which destabilizes the coating bead. Therefore, the defect swelling occurs at lower wet film thicknesses. For diverging angle of attack $\alpha < 0$, the opposite effect on the upstream side and a higher pressure drop below the downstream slot-die lip stabilize the coating bead. This is consistent with the results of Lee et al.^[26] The result is a decreasing upper process limit with an increasing angle of attack α in which stable coatings can be produced.

2.2.2. Edge Formation

The dimensionless edge height H^* for different electrode coatings at a constant coating speed of 10 m min^{-1} and a constant dimensionless gap G^* of 1.15 is shown in Figure 8 as a function of the angle of attack α .

The dimensionless edge height H^* of the wet film decreases with increasing angle of attack α of the slot die (diverging $< 0 <$ converging) for all the investigated electrode thicknesses. For converging angle of attack $\alpha > 0$, edge elevations can be reduced. For diverging angle of attack $\alpha < 0$, the opposite effect was observed. Considering the standard deviation, the dimensionless edge height H^* is shifted to higher values for thicker electrode coatings ($h_{\text{wet}} = 365 \mu\text{m}$ and $h_G = 420 \mu\text{m}$) compared with thinner electrode coatings ($h_{\text{wet}} = 156 \mu\text{m}$ and $h_G = 180 \mu\text{m}$) for constant angle of attack α with the exception of values for a diverging angle of attack α of -1.5° . With decreasing angle of attack α , the standard deviation of the experimental data increases. Lee et al. found that free-surface oscillation at the downstream meniscus is enhanced by diverging angle of attack, whereas the free-surface oscillation at the downstream meniscus tends to be damped at converging angle of attack.^[25] The edge elevation for high-capacity electrode coatings ($h_{\text{wet}} = 260 \mu\text{m}$ and $h_G = 300 \mu\text{m}$)

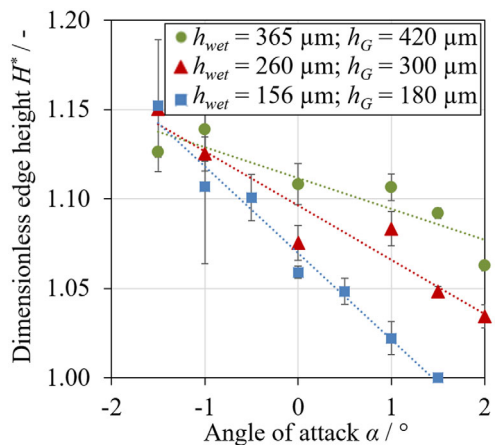


Figure 8. Dimensionless edge height H^* for different electrode coatings as a function of the angle of attack α . Experimental data of state-of-the-art electrode coatings ($h_{\text{wet}} = 156 \mu\text{m}$ and $h_G = 180 \mu\text{m}$, blue squares), high-capacity electrode coatings ($h_{\text{wet}} = 260 \mu\text{m}$ and $h_G = 300 \mu\text{m}$, red triangles), and ultrathick high-capacity electrode coatings ($h_{\text{wet}} = 365 \mu\text{m}$ and $h_G = 420 \mu\text{m}$, green dots) are compared for a coating speed of 10 m min^{-1} and a dimensionless coating gap G^* of 1.15 (for electrode configurations, see Table 1).

was reduced from $18.6 \mu\text{m}$ for the standard setting without angle of attack α by 34% to $12.3 \mu\text{m}$ for a setting with an angle of attack α of 1.5° . For ultrathick high-capacity electrode coatings ($h_{\text{wet}} = 365 \mu\text{m}$ and $h_G = 420 \mu\text{m}$), the edge elevation of the wet film was reduced from $29.9 \mu\text{m}$ for a setting without angle of attack α by 32% to $20.4 \mu\text{m}$ for a setting with an angle of attack α of 1.5° . For state-of-the-art electrode coatings ($h_{\text{wet}} = 156 \mu\text{m}$ and $h_G = 180 \mu\text{m}$), the edge elevations were eliminated by setting an angle of attack α of 1.5° . The superposition of several mechanisms could be responsible for these results. On the one hand, the lower pressure drop below the upstream slot-die lip in combination with the decreasing capillary pressure for converging angle of attack α could counteract edge formation effects such as neck-in flow and surface tension. On the other hand, the pressure drop below the downstream slot-die lip is higher than the pressure drop below the upstream slot-die lip, which can lead to an increasing widening of the coating. For diverging angle of attack α , the opposite effect could lead to an increasing dimensionless edge height H^* . Especially, an increasing dimensionless coating gap G^* in x -direction in the case of diverging angle of attack α increases the draw ratio. Thus, the neck-in flow increases, which leads to increasing edge elevations during slot-die coating. This is already known from literature and the results are in Section 2.1.^[10,15,19,23]

Using an angle of attack α of 2° for high-capacity electrode coatings and ultrathick high-capacity electrode coatings, a reduction of the dimensionless edge height H^* is possible, but a further reduction of the coating gap h_G is unfeasible. The maximum wet film thickness h_{wet} for coating gaps for high-capacity electrode coatings ($h_G = 300 \mu\text{m}$) is $\approx 265 \mu\text{m}$ ($G^* \approx 1.13$). This is very close to the wet film thickness $h_{\text{wet}} = 260 \mu\text{m}$, which is required to reach the area capacity of 5 mAh cm^{-2} . Thus, a further adjustment of the dimensionless coating gap G^* could lead to swelling

due to excessive substrate thickness variations. The same fact is valid for ultrathick high-capacity electrode coatings. For the set coating gap h_G of $420 \mu\text{m}$, the resulting maximum wet film thickness h_{wet} is $\approx 373 \mu\text{m}$, which is close to the wet film thickness $h_{\text{wet}} = 365 \mu\text{m}$ for the required area capacity of 7 mAh cm^{-2} . Therefore, the value of interest is the angle of attack α of 1.5° . This operation point offers potential for an optimization of the edge formation with combined influences of dimensionless gap G^* and angle of attack α for high-capacity electrode coatings.

Further, the edge width b_{edge} (Figure 9a) and the widening during the coating process b_{widening} (Figure 9b) for different electrode coatings are shown in Figure 7 as a function of the angle of attack α .

The edge width b_{edge} (Figure 9a) of the wet film slightly decreases with increasing angle of attack α for all the electrode thicknesses. The experimental values of edge width b_{edge} are shifted approximately in parallel to higher values for thicker electrode coatings. In contrast, the widening of the coating during the coating process b_{widening} (Figure 9b) increases with

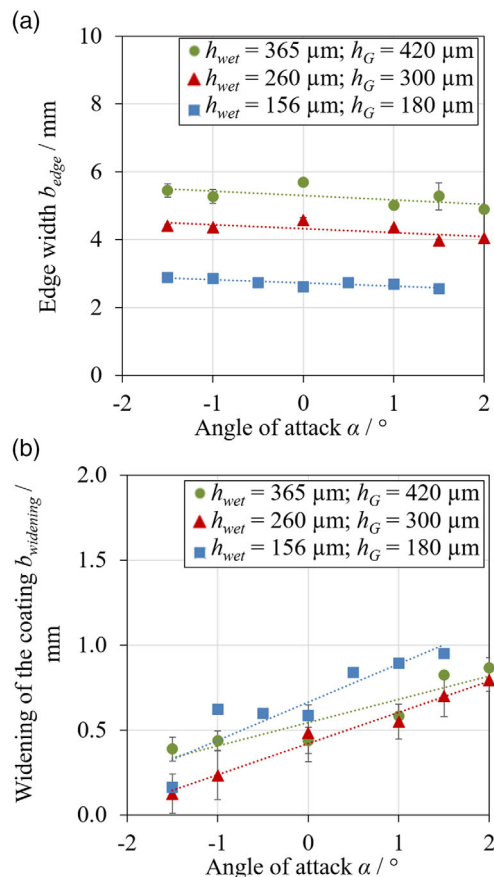


Figure 9. a) Edge width b_{edge} and b) widening during the coating process b_{widening} for different electrode coatings as a function of the angle of attack α . Experimental data of state-of-the-art electrode coatings ($h_{\text{wet}} = 156 \mu\text{m}$ and $h_G = 180 \mu\text{m}$, blue squares), high-capacity electrode coatings ($h_{\text{wet}} = 260 \mu\text{m}$ and $h_G = 300 \mu\text{m}$, red triangles), and ultrathick high-capacity electrode coatings ($h_{\text{wet}} = 365 \mu\text{m}$ and $h_G = 420 \mu\text{m}$, green dots) are compared for a coating speed of 10 m min^{-1} and a dimensionless coating gap G^* of 1.15 (for electrode configurations, see Table 1).

increasing angle of attack α . However, in addition to reducing the draw ratio, the widening of the coating b_{widening} has an additional influence on edge formation. The effect of the widening ensures that the edge elevation is distributed over a wider area in cross-web direction. Due to mass conservation, the widening of the coating counteracts the edge formation effects such as neck-in flow and surface tension. This is supported by the fact that with increasing widening b_{widening} , the dimensionless edge height H^* decreases.

2.3. Optimized Setup for Ultrathick Electrode Coatings

The dimensionless edge height H^* for different electrode coatings is shown in **Figure 10** as a function of the dimensionless coating gap G^* at a constant coating speed of 10 m min^{-1} and with optimized converging angle of attack α of 1.5° (see Section 2.2.2).

As expected from the study of the influence of the dimensionless coating gap G^* on edge formation (Section 2.1), the dimensionless edge height H^* of the wet film decreases with decreasing dimensionless coating gap G^* . As already described in Section 2.1, the experimental data are shifted approximately in parallel to higher values for increasing electrode thickness comparing constant dimensionless coating gaps G^* . With this setting, the dimensionless edge height H^* of high-capacity electrode coatings and ultrathick high-capacity electrode coatings can be strongly reduced. Considering the results of the investigation of the process limits (Section 2.2.1), the dimensionless coating gap G^* was set to 1.05. For high-capacity electrode coatings ($h_{\text{wet}} = 260 \mu\text{m}$), the edge elevations of the wet film are reduced from $12.3 \mu\text{m}$ for a setting with a dimensionless coating gap G^* of 1.17 by 53% to $5.8 \mu\text{m}$ for a setting with G^* of 1.05. For ultrathick high-capacity electrode coatings ($h_{\text{wet}} = 365 \mu\text{m}$), the edge elevations are reduced from $20.4 \mu\text{m}$ for a setting with a dimensionless coating gap G^* of 1.18 by 24% to $15.5 \mu\text{m}$ for a setting with G^* of 1.03. The positive effects of the influence of

decreasing dimensionless coating gap G^* and, in addition, the set converging angle of attack α of 1.5° ensure that the combination of a lower draw ratio, lower pressure drop below the die lips as well as lower capillary pressure, and, in addition, the widening of the coating b_{widening} lead to lower dimensionless edge heights. Increasing the dimensionless coating gap G^* has the opposite effect. For high-capacity electrode coatings ($h_{\text{wet}} = 260 \mu\text{m}$), the edge elevations of the wet film are increased from $12.3 \mu\text{m}$ (setting with a dimensionless coating gap G^* of 1.17) by 57% to $19.3 \mu\text{m}$ (setting with G^* of 1.41). For ultrathick high-capacity electrode coatings ($h_{\text{wet}} = 365 \mu\text{m}$), the edge elevations are increased from $20.4 \mu\text{m}$ (setting with a dimensionless coating gap G^* of 1.18) by 82% to $37.1 \mu\text{m}$ (setting with G^* of 1.03).

As an overview, the dimensionless edge height H^* for different electrode coatings is shown in **Figure 11** as a function of different process settings.

For state-of-the-art electrode coatings ($h_{\text{wet}} = 156 \mu\text{m}$ for 2.2 mAh cm^{-2}), it is possible to eliminate edge elevations during slot-die coating using a setting with a converging angle of attack α of 1.5° and a dimensionless coating gap G^* of 1.15. In addition, for high-capacity electrode coatings ($h_{\text{wet}} = 260 \mu\text{m}$ for 5 mAh cm^{-2}), a strong reduction of edge elevations from $18.6 \mu\text{m}$ by 34% to $12.3 \mu\text{m}$ and for ultrathick high-capacity electrode coatings ($h_{\text{wet}} = 365 \mu\text{m}$ for 7 mAh cm^{-2}) from $29.9 \mu\text{m}$ by 32% to $20.4 \mu\text{m}$ by setting a converging angle of attack α of 1.5° is possible. Using the optimized process settings, which combine the advantageous effects of single-process parameters (converging angle of attack α of 1.5° and dimensionless coating gap G^* of 1.05), it is possible to strongly reduce edge elevations of the wet film for high-capacity electrode coatings ($h_{\text{wet}} = 260 \mu\text{m}$ for 5 mAh cm^{-2}) by 69% to $5.8 \mu\text{m}$ compared with the standard coating process (without angle of attack and dimensionless coating gap G^* of 1.15). Using the optimized setup, even for ultrathick high-capacity electrode coatings ($h_{\text{wet}} = 365 \mu\text{m}$ for

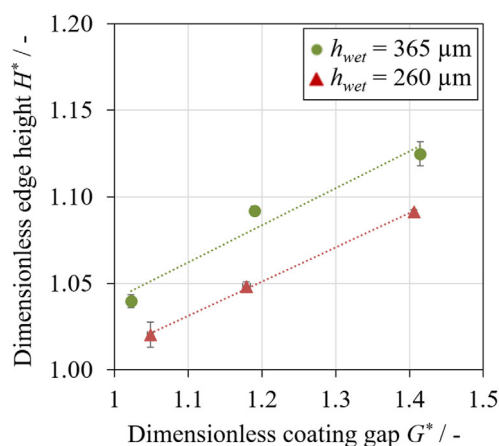


Figure 10. Dimensionless edge height H^* for different electrode coatings as a function of the dimensionless coating gap G^* . Experimental data for high-capacity electrode coatings ($h_{\text{wet}} = 260 \mu\text{m}$, red triangles) and ultrathick high-capacity electrode coatings ($h_{\text{wet}} = 365 \mu\text{m}$, green dots) are compared for a coating speed of 10 m min^{-1} and a converging angle of attack α of 1.5° (for electrode configurations, see Table 1).

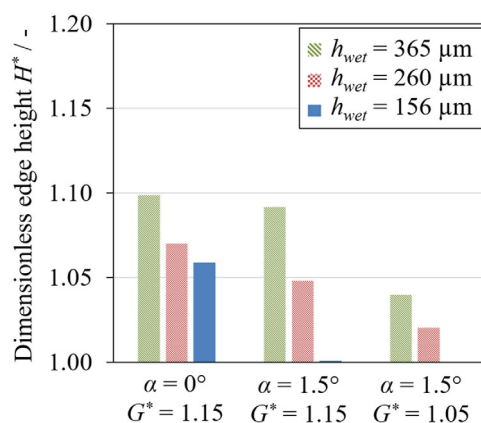


Figure 11. Dimensionless edge height H^* for different electrode coatings as a function of different process settings. Experimental data of state-of-the-art electrode coatings ($h_{\text{wet}} = 156 \mu\text{m}$ for 2.2 mAh cm^{-2} , blue bars), high-capacity electrode coatings ($h_{\text{wet}} = 260 \mu\text{m}$ for 5 mAh cm^{-2} , red dotted bars), and ultrathick high-capacity electrode coatings ($h_{\text{wet}} = 365 \mu\text{m}$ for 7 mAh cm^{-2} , green striped bars) are compared for a coating speed of 10 m min^{-1} (for electrode configurations, see Table 1).

7 mAh cm⁻²), a strong reduction of edge elevations by 48% to 15.5 μm compared with the standard coating process is possible.

3. Conclusion

One of the main challenges in processing high-capacity battery cells with ultrathick electrodes is the edge formation at the lateral edges during the coating step. Edge elevations could lead to defects in subsequent process steps, especially during winding and calendaring of dry electrodes. In addition, cutting off defects or edge elevations of the electrodes are a responsible part of high reject rates in the process chain. Therefore, it is necessary to eliminate edge elevations in the wet film during slot-die coating step of the electrode production chain.

In this contribution, a systematic investigation of the influence of process parameters on edge formation during the coating step and optimization, which combines different influences of process parameters, is presented. It was shown that the dimensionless edge height of the wet film decreases with decreasing dimensionless gap for all the investigated electrode thicknesses. As known from literature, using a setting with a dimensionless coating gap of 1, the elimination of edge elevations during slot-die coating for state of the art and very thin electrode coatings is possible. In addition, for high-capacity and ultrathick high-capacity electrode coatings, a reduction of edge elevations is possible. Since the setting of the dimensionless coating gap to 1 is in contrast to the best coating stability, the influence of the angle of attack of the slot die on edge formation was investigated. It was shown that the dimensionless edge height of the wet film decreases with increasing angle of attack from negative diverging angles to positive converging angles. At first, a setting with angle of attack of 1.5° was compared with the standard coating process without angle of attack. For this setting, the edge elevations of high-capacity electrode coatings ($h_{\text{wet}} = 260 \mu\text{m}$ for 5 mAh cm⁻²) were reduced from 18.6 μm by 34% to 12.3 μm and for ultrathick high-capacity electrode coatings ($h_{\text{wet}} = 365 \mu\text{m}$ for 7 mAh cm⁻²), edge elevations were reduced from 29.9 μm by 32% to 20.4 μm. For this setting, edge elevations of the wet film for high-capacity electrode coatings and ultrathick high-capacity electrode coatings are still relevant.

Consequently, an optimized coating setup with a converging angle of attack of 1.5° and a dimensionless coating gap of 1.05 was investigated and compared with the standard coating process (no angle of attack and dimensionless coating gap of 1.15). For high-capacity electrode coatings ($h_{\text{wet}} = 260 \mu\text{m}$ for 5 mAh cm⁻²), edge elevations are strongly reduced by 69% to 5.8 μm. With this setup, a strong reduction of edge elevations of the wet film is even possible for ultrathick high-capacity electrode coatings ($h_{\text{wet}} = 365 \mu\text{m}$ for 7 mAh cm⁻²) by 48% to 15.5 μm.

The investigated process parameters can help significantly reduce reject in the industrial roll-to-roll process of manufacturing high-capacity electrodes. The combination of the advantages of the dimensionless coating gap and the angle of attack are a promising way to eliminate edge elevations during the coating step for a wide range of industrially relevant electrode thicknesses.

4. Experimental Section

Slurry Preparation: A water-based graphite anode slurry was prepared for the experiments using a planetary mixer (Inoue Manufacturing Inc.). A solid content of 43% was set. The composition of the graphite anode slurry is shown in Table 2.

Initially, a flake graphite (SMG-A, Hitachi Chemical Co., Ltd.) was mixed with carbon black (Super C65, Timcal) in a dry mixing step. Deionized water and carboxymethyl cellulose (CMC) solution (Sunrose CMC MAC500LC, Nippon Paper Industries) were added in three separate kneading steps. The kneading time of the different steps was 10, 30, and 120 min. Finally, styrene-butadiene rubber (SBR) dispersion (BM-400, Zeon Corporation) was added.

Viscosity was measured using a rotational rheometer (Anton Paar) with a plate-plate geometry. The plate diameter was 25 mm in each case. As shown in **Figure 12**, the viscosity was plotted as a function of the shear rate from 10 to 1000 s⁻¹. The experimental data points are marked with blue dots and the power law fit is shown as a blue line. The relevant shear rate range for slot-die coating is marked with dashed lines.

The viscosity curve shows a shear-thinning behavior. In the diagram, the Power-Law parameters are shown with the corresponding fit describing the experimental data. For the experiments, there was a relevant shear rate range of 397–926 s⁻¹ for the used coating gaps and coating speed (dashed line). The surface tension was in the range of the solvent water about 66–68 mN m⁻¹.

Experimental Coating Setup: To investigate the coating process independently from the drying process, coating experiments were performed on a Development Coater (TSE Troller AG). A slot die was mounted on a high-precision steel roller in 8 o'clock position to the center of the roller. The coating setup and the measurement methods are schematically shown in **Figure 13**.

With this experimental setup, precise coating gaps between slot die and steel roller could be adjusted. The diameter of the steel roller was 300 mm and the concentricity inaccuracy was < 1 μm. The coating gap for each angle of attack was set on the lowest point of the slot-die lips via polyethyleneterephthalat shims to 180, 300, and 420 μm. The slot width of the slot die was adjusted to 500 μm using a spacer shim and the die outlet width was set to 50 mm. With the experimental setup, different angles of attack between -1.5° and 2° were adjusted in 0.5° steps. In the experimental study, a coating speed of 10 m min⁻¹ was set. Previous investigations showed no influence of the coating speed on the dimensionless edge height.^[1,15] In all the experiments, the volume flow and, thus, the wet film thickness were adjusted using a high-precision syringe pump (Cetoni neMESYS).

Film Characterization Methods: The film height profile of each edge was measured using a laser triangulation system (Keyence LJ-V). The laser

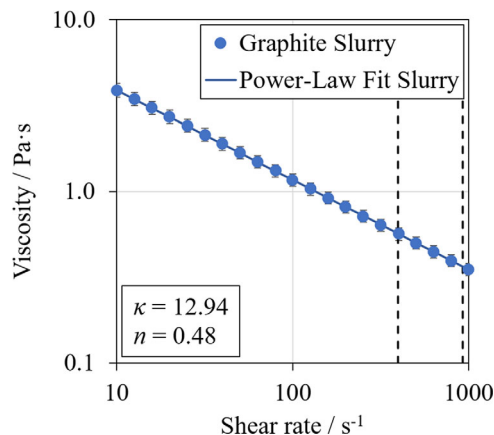


Figure 12. Viscosity as a function of the shear rate. Experimental data (blue dots) and the power-law fit of the slurry are compared for a shear rate range of 10–1000 s⁻¹.

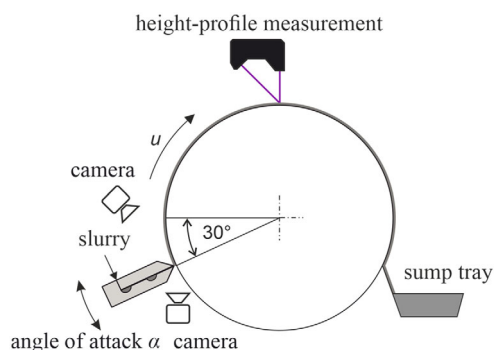


Figure 13. Schematic illustration of the coating setup and measurement methods.

triangulation sensors had a measuring width of 16 mm. Using two sensors, one at each edge of the coating, allowed very precise control of the crossweb profile of the film. To eliminate periodic effects on the wet film profile, the duration of measurements was chosen to cover a multiple of a full roller revolution. In addition, the spatial sampling rate was increased by adjusting the measuring frequency. The height profile data of both the coating edges was then analyzed. Therefore, three measurements were taken of both lateral edges. In addition, the wet film width was determined from image data taken with a camera placed above the slot die. The stability of the upstream meniscus and, thus, the maximum wet film thickness was identified from video data taken with a micro-universal serial bus camera. This camera was placed below the slot die and the upstream meniscus was recorded.

Acknowledgements

The authors would like to acknowledge financial support from the Federal Ministry of Education and Research (BMBF) via the ProZell cluster project “HiStructures” (grant number: 03XP0243C). This work contributes to the research conducted at the Center for Electrochemical Energy Storage Ulm & Karlsruhe (CELEST).

Open Access funding enabled and organized by Projekt DEAL.

Conflict of Interest

The authors declare no conflict of interest.

Data Availability Statement

The data that support the findings of this study are available from the corresponding author upon reasonable request.

Keywords

edge formation, electrode production, high-capacity electrodes, lithium-ion batteries, slot-die coating

Received: June 30, 2022
Revised: August 26, 2022
Published online:

- [1] S. Spiegel, T. Heckmann, A. Altvater, R. Diehm, P. Scharfer, W. Schabel, *J. Coat. Technol. Res.* **2022**, *19*, 121.
- [2] G. Patry, A. Romagny, S. Martinet, D. Froelich, *Energy Sci. Eng.* **2015**, *3*, 71.
- [3] D. L. Wood, J. Li, C. Daniel, *J. Power Sources* **2015**, *275*, 234.
- [4] M. Müller, L. Pfaffmann, S. Jaiser, M. Baunach, V. Trouillet, F. Scheiba, P. Scharfer, W. Schabel, W. Bauer, *J. Power Sources* **2017**, *340*, 1.
- [5] M. Baunach, S. Jaiser, S. Schmelzle, H. Nirschl, P. Scharfer, W. Schabel, *Drying Technol.* **2016**, *34*, 462.
- [6] S. Jaiser, J. Kumberg, J. Klaver, J. L. Urai, W. Schabel, J. Schmatz, P. Scharfer, *J. Power Sources* **2017**, *345*, 97.
- [7] S. Jaiser, M. Müller, M. Baunach, W. Bauer, P. Scharfer, W. Schabel, *J. Power Sources* **2016**, *318*, 210.
- [8] J. Kumberg, M. Müller, R. Diehm, S. Spiegel, C. Wachsmann, W. Bauer, P. Scharfer, W. Schabel, *Energy Technol.* **2019**, *7*, 1900722.
- [9] Z. Du, K. M. Rollag, J. Li, S. J. An, M. Wood, Y. Sheng, P. P. Mukherjee, C. Daniel, D. L. Wood, *J. Power Sources* **2017**, *354*, 200.
- [10] M. Schmitt, P. Scharfer, W. Schabel, *J. Coat. Technol. Res.* **2014**, *11*, 57.
- [11] J. Klemens, L. Schneider, E. C. Herbst, N. Bohn, M. Müller, W. Bauer, P. Scharfer, W. Schabel, *Energy Technol.* **2022**, *10*, 2100985.
- [12] R. Sahore, D. L. Wood, A. Kukay, K. M. Grady, J. Li, I. Belharouak, *ACS Sustainable Chem. Eng.* **2020**, *8*, 3162.
- [13] *Handbuch Lithium-Ionen-Batterien* (Ed: R. Korthauer), Springer Berlin Heidelberg, Berlin, Heidelberg, s.l. **2013**.
- [14] J. C. Eser, T. Wirsching, P. G. Weidler, A. Altvater, T. Börnhorst, J. Kumberg, G. Schöne, M. Müller, P. Scharfer, W. Schabel, *Energy Technol.* **2020**, *8*, 1801162.
- [15] M. Schmitt, *Slot Die Coating of Lithium-Ion Battery Electrodes*, KIT Scientific Publishing, Karlsruhe, Germany **2016**.
- [16] S. F. Kistler, P. M. Schweizer, *Liquid Film Coating. Scientific Principles and their Technological Implications*, Springer Netherlands, Dordrecht **2012**.
- [17] F. Durst, H.-G. Wagner, in *Liquid Film Coating. Scientific Principles and their Technological Implications* (Eds: S. F. Kistler, P. M. Schweizer), Springer Netherlands, Dordrecht **2012**, pp. 401–426.
- [18] S. Kim, J. Lee, C. Lee, *Int. J. Adv. Manuf. Technol.* **2019**, *104*, 2991.
- [19] E. B. Gutoff, E. D. Cohen, G. I. Kheboian, *Coating and Drying Defects. Troubleshooting Operating Problems*, Wiley-Interscience, Hoboken, NJ **2006**.
- [20] T. Günther, D. Schreiner, A. Metkar, C. Meyer, A. Kwade, G. Reinhart, *Energy Technol.* **2020**, *8*, 1900026.
- [21] R. Diehm, H. Weinmann, J. Kumberg, M. Schmitt, J. Fleischer, P. Scharfer, W. Schabel, *Energy Technol.* **2019**, *5*, 1900137.
- [22] M. Schmitt, R. Diehm, P. Scharfer, W. Schabel, *J. Coat. Technol. Res.* **2015**, *12*, 927.
- [23] T. Dobroth, L. Erwin, *Polym. Eng. Sci.* **1986**, *26*, 462.
- [24] G. H. Han, S. H. Lee, W.-G. Ahn, J. Nam, H. W. Jung, *J. Coat. Technol. Res.* **2014**, *11*, 19.
- [25] S. Lee, J. Nam, *AIChE J.* **2015**, *61*, 1745.
- [26] S. H. Lee, S. J. Kim, J. Nam, H. W. Jung, J. C. Hyun, *J. Coat. Technol. Res.* **2014**, *11*, 47.
- [27] O. J. Romero, L. E. Scriven, M. S. Da Carvalho, *AIChE J.* **2006**, *52*, 447.
- [28] S. M. Raupp, M. Schmitt, A.-L. Walz, R. Diehm, H. Hummel, P. Scharfer, W. Schabel, *J. Coat. Technol. Res.* **2018**, *15*, 899.